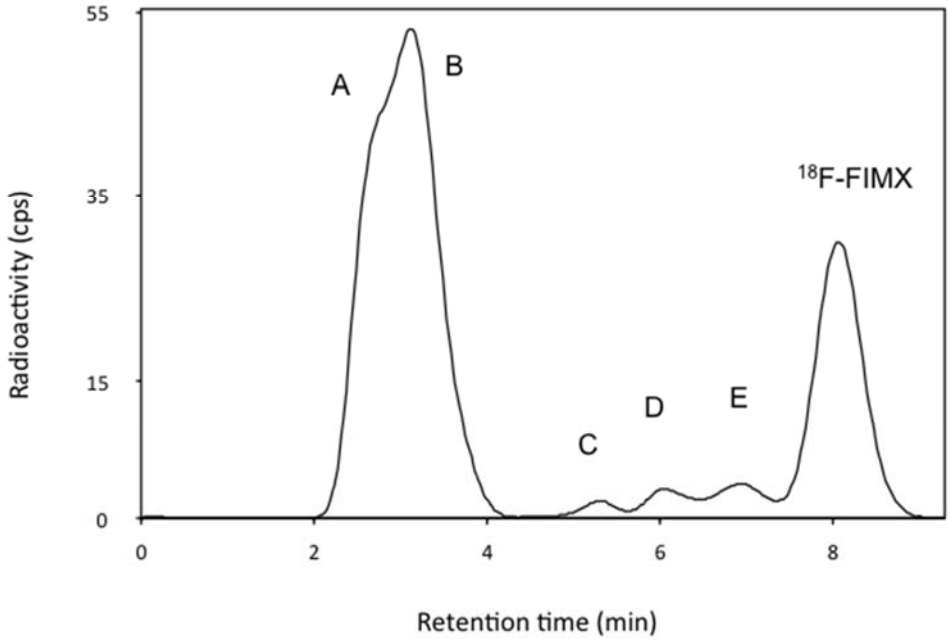

Supplemental Fig 1: Human plasma sample at 60 minutes after intravenous injection of ^{18}F-FIMX (189 MBq). The approximate concentration of radiometabolites was: A = 22.5%; B = 45.2%; C = 1.2%; D = 2.4%; E = 3.2%; and parent = 25.4%. The radiopeaks of A and B were not well resolved, and the presence of more radiometabolites cannot be ruled out. ^{18}F-FIMX eluted at eight minutes and was well separated from its radiometabolites. Radioanalysis was done on a C_{18}-reverse phase HPLC column (XTerra, 10 µm, 7.8 x 300 mm; Waters Corp.; Milford, MA) and eluted at 5.0 mL/min with methanol : water : triethylamine (65:35:0.1 by vol.) as previously described *(1)*.

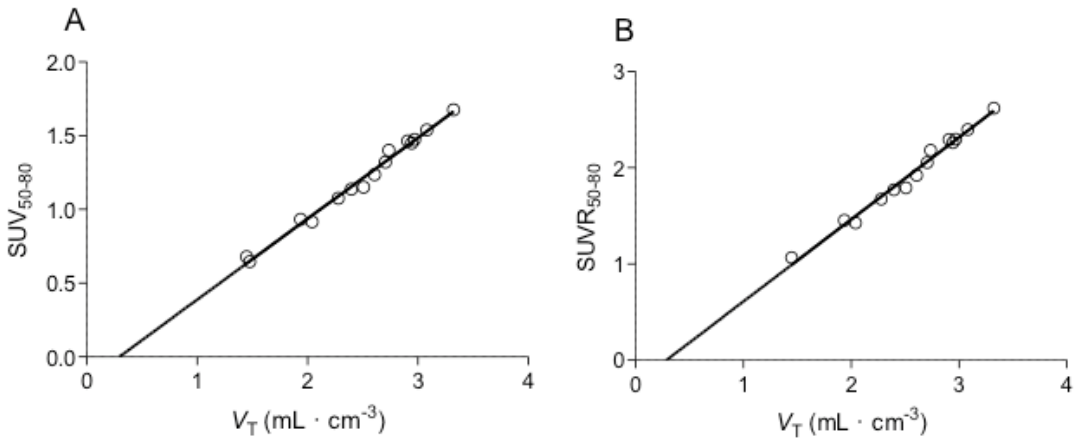

Supplemental Fig 2: Linear regression analysis between the two-tissue compartment model-distribution volume (V_T) values of ^{18}F-FIMX measured with a metabolite-corrected input function, and standard uptake value measured from 50 to 80 minutes (SUV_{50-80}) (A) or the ratio of SUV over the caudate in the same time interval ($SUVR_{50-80}$) (B) . Both lines use the same brain regions, except that the caudate, used as a reference region, is missing from (B). The equation of the SUV_{50-80} line is y = 0.549x - 0.161; R^2= 0.989. The equation of the $SUVR_{50-80}$ line is y = 0.853x - 0.244; R^2= 0.983.

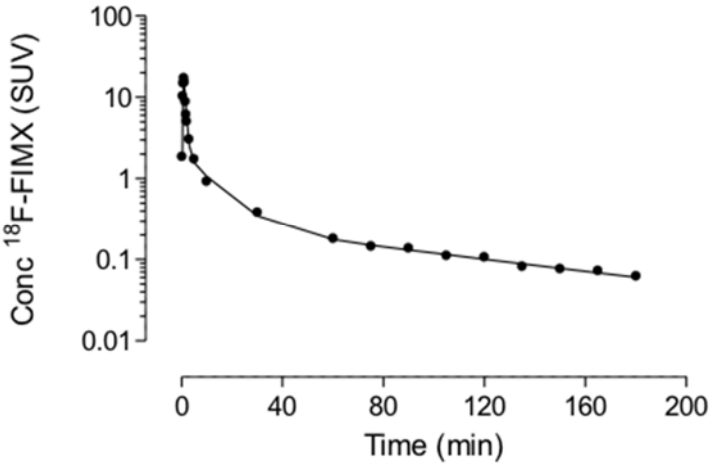

Supplemental Fig 3: Metabolite-corrected arterial input function acquired over 180 minutes in a monkey, fitted with a tri-exponential function.

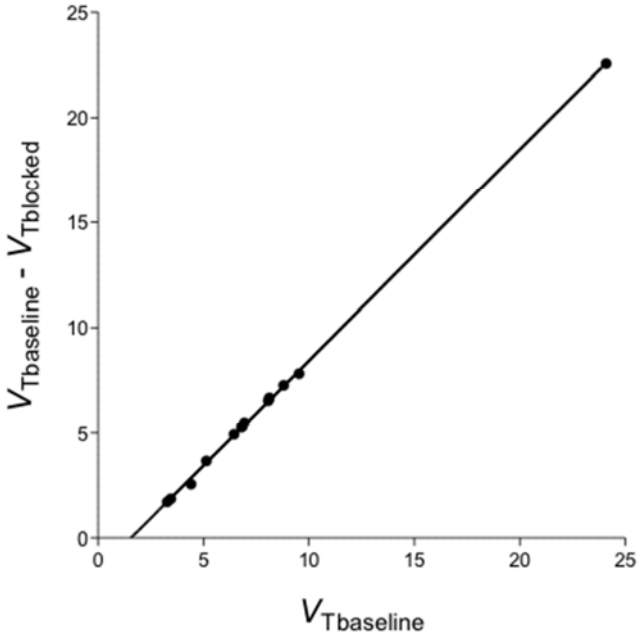

Supplemental Fig 4: Lassen plot of monkey brain data. The baseline distribution volume (V_T) values are on the *x*-axis, and the specific binding (baseline V_T minus the nonspecific binding measured from the blocked scan) is on the *y*-axis. The equation of the line is y = 1.003x - 1.576; R^2 = 0.9995. The *x*-intercept is 1.57.

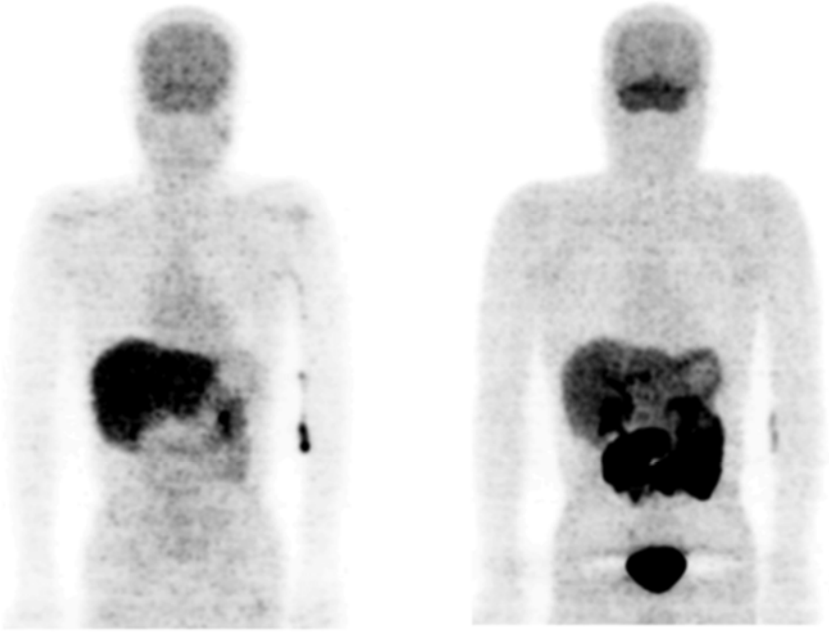

Supplemental Fig 5: Whole body biodistribution of ^{18}F-FIMX at an early time (~10 minutes) and a later time (~100 minutes) after injection, shown in maximum-intensity projection. At ~10 minutes, the organs with a high blood pool (especially the liver) are clearly visible. At ~100 minutes, radioactivity from either parent or radiometabolites was excreted via the urinary and hepatobiliary systems. The high uptake in the cerebellum also gradually became evident.

Supplemental Table 1. Kinetic rate constants measured with a two-tissue compartment model and a 120-minute scan from 12 subjects

Region	K_1 (mL • cm^{-3} • min^{-1})	k_2 (min^{-1})	k_3 (min^{-1})	k_4 (min^{-1})
Frontal Cortex	0.12 (2.6%)	0.16 (12.7%)	0.23 (19.2%)	0.09 (5.5%)
Temporal Cortex	0.12 (2.6%)	0.12 (11.0%)	0.16 (21.0%)	0.07 (5.4%)
Hippocampus	0.09 (3.0%)	0.11 (14.0%)	0.11 (16.5%)	0.05 (5.5%)
Anterior Cingulum	0.12 (2.2%)	0.13 (13.4%)	0.20 (21.6%)	0.08 (5.9%)
Caudate	0.11 (4.6%)	0.23 (17.8%)	0.20 (21.5%)	0.09 (6.4%)
Putamen	0.14 (3.7%)	0.23 (14.1%)	0.18 (14.7%)	0.08 (4.1%)
Thalamus	0.12 (2.4%)	0.13 (12.6%)	0.16 (15.6%)	0.06 (4.8%)
Cerebellum	0.13 (1.1%)	0.03 (7.3%)	0.03 (17.1%)	0.02 (14.4%)

Rate constants are the median value measured with a two-tissue compartment model and a 120-minute scan from 12 subjects. The median standard errors are in parentheses and are expressed as the percentage of the variable

Supplemental Table 2. Total distribution volume (mL • cm^{-3}) calculated from compartmental modeling, the Logan plot, MA1, MA2, RE-GP, SA, and RSSA at the regional level for a 120-minute scan

Region	Unconstrained Two-tissue	Logan	MA1	MA2	RE-GP	SA	RSSA
Frontal Cortex	2.39 (0.31)	2.38 (0.31)	2.38 (0.31)	2.40 (0.32)	2.39 (0.31)	2.35 (0.32)	2.32 (0.35)
Temporal Cortex	3.08 (0.37)	3.05 (0.36)	3.02 (0.36)	3.06 (0.37)	3.07 (0.37)	3.13 (0.39)	3.03 (0.40)
Hippocampus	2.91 (0.39)	2.90 (0.40)	2.87 (0.40)	2.93 (0.42)	2.94 (0.41)	3.04 (0.45)	2.91 (0.38)
Anterior Cingulum	2.94 (0.41)	2.90 (0.40)	2.88 (0.39)	2.91 (0.40)	2.92 (0.40)	2.93 (0.45)	2.88 (0.42)
Caudate	1.48 (0.17)	1.50 (0.17)	1.53 (0.19)	1.49 (0.17)	1.51 (0.17)	1.39 (0.16)	1.45 (0.18)
Putamen	2.04 (0.25)	2.06 (0.26)	2.06 (0.27)	2.08 (0.28)	2.06 (0.26)	1.99 (0.27)	1.98 (0.28)
Thalamus	3.32 (0.50)	3.28 (0.49)	3.25 (0.48)	3.31 (0.49)	3.31 (0.49)	3.43 (0.51)	3.31 (0.51)
Cerebellum	11.0 (1.9)	9.95 (1.70)	9.08 (1.50)	10.6 (1.71)	10.5 (1.74)	10.1 (1.63)	8.84 (1.41)

Data are expressed in mean ± (SD)

With compartmental modeling, the distribution volume in the cerebellum for a 210-minute scan is 13.4 ± 2.2.

Abbreviations: MA: Ichise's multilinear analysis; SA: standard spectral analysis; RE-GP: Zhou's relative-equilibrium Gjedde-Patlak bi-graphical analysis; RSSA: rank-shaping spectral analysis.

Supplemental Table 3: Coefficient of variation using different invasive and non-invasive techniques in selected regions

Region	V_T	V_T/f_p	BP_{ND}	SUV_{50-80}	$SUVR_{50-80}$
Cerebellum	17.6	22.9	9.76	18.0	13.2
Thalamus	14.9	24.3	14.5	20.3	11.1
Hippocampus	13.4	20.4	17.9	19.4	10.4
Frontal	13.0	22.2	20.3	21.5	9.42
Temporal	12.0	21.6	15.5	21.4	9.90
Average	13.2	23.0	19.8	21.2	9.90

Data are presented as coefficients of variation (= standard deviation / mean × 100%).
The caudate was used as the reference region for $SUVR_{50-80}$ and BP_{ND}.
V_T/f_P = total distribution volume/free fraction of radioligand; $SUV(R)_{50-80}$ = standardized uptake value (ratio) measured in the interval 50-80 minutes; BP_{ND} = binding potential over the non-displaceable compartment, measured by simplified reference tissue model (SRTM).

Supplemental Table 4: Residence times for source organs

Organ	Residence Time (hours)
Brain	0.087 ± 0.010
Gall bladder	0.121 ± 0.084
Heart wall	0.020 ± 0.003
Kidneys	0.062 ± 0.013
Liver	0.226 ± 0.007
Lungs	0.014 ± 0.001
Marrow	0.034 ± 0.009
Spleen	0.003 ± 0.000
Remainder in body	1.16 ± 0.01

Values are mean ± SD for four healthy subjects

Supplemental Table 5. Radiation dosimetry estimates for ^{18}F-FIMX in the standard anthropomorphic phantom for the adult man

Organ	Radiation dose	
	µSv/MBq	mrem/mCi
Adrenals	11.1	40.8
Brain	16.4	60.5
Breasts	5.4	19.8
Gallbladder Wall	245	909
Lower Large Intestine Wall	14.0	51.8
Small Intestine	11.9	43.9
Stomach Wall	8.8	32.7
Upper Large Intestine Wall	12.6	46.6
Heart Wall	16.2	59.9
Kidneys	42.2	156
Liver	35.2	130
Lungs	6.9	25.6
Muscle	8.3	30.6
Ovaries	14.0	51.7
Pancreas	12.2	45.1
Red Marrow	10.1	37.2
Osteogenic Cells	11.4	42.2
Skin	5.5	20.2
Spleen	8.8	32.6
Testes	10.2	37.6
Thymus	6.4	23.9
Thyroid	6.1	22.5
Urinary Bladder Wall*	251	931
Uterus	22.8	84.4
Total Body	9.5	35.0
Effective dose	23.4	86.6

*Value obtained from the dynamic bladder model using a voiding interval of 2.4 hours

Supplemental Methods

According to the protocol previously established to assess the radiation safety of ^{18}F-labeled PET tracers for first-in-human studies *(2)*, we first acquired a whole-body scan in a 22-year old healthy male volunteer after injecting a low activity of ^{18}F-FIMX (74 MBq). We then acquired dynamic brain images in the 12 healthy subjects for kinetic modeling (189 ± 3 MBq), consisting of a 120-minute scan subdivided into 33 frames of increasing length (from 30 seconds to five minutes). For six of these 12 subjects, the scan was prolonged to 210 minutes after a 30-minute pause. These 12 subjects also underwent brain magnetic resonance imaging (MRI) to delineate anatomical brain structures.

Analysis of Brain Images: Methods

MRI brain images were segmented using FreeSurfer 5.3.0 (http://surfer.nmr.mgh.harvard.edu) to obtain individual atlases comprising 16 regions (cerebellum, caudate, putamen, thalamus, hippocampus, amygdala, insula, anterior and posterior cingulum, precuneus, frontal, temporal, parietal and occipital cortex, brainstem, and white matter). Each region was obtained from the average of the left and right region, weighted by volume. The PET images were then co-registered to the FreeSurfer's output MRIs using SPM5 (Statistical Parametric Mapping, Wellcome Department of Cognitive Neurology, London, UK).

Quantification of ^{18}F-FIMX binding: Methods

V_T was calculated using compartmental modeling as well as non-compartmental models. Both one- and two-tissue compartment models were used. The individual rate constants (K_1, k_2, k_3, and k_4) were estimated using the weighted least-square method with the Marquardt optimizer. Brain data were weighted frame-wise by assuming that the inverse square root of noise-equivalent counts was proportional to the normalized standard deviation of each frame. The arterial whole blood curve was used to correct brain data for the vascular component, assuming that the blood volume represents 5% of the total brain volume. The delay between the arrival of the radioligand to the brain and to the radial artery was estimated by fitting the curve of the whole brain, minus the white matter.

Non-compartmental models: In order to assess the performance of alternative models to quantify ^{18}F-FIMX at the region level, we calculated V_T using the Logan graphical analysis *(3)*, Ichise's multilinear analysis MA1 *(4)* and MA2 *(4)*, Zhou's Relative-Equilibrium Gjedde-Patlak bi-graphical analysis (RE-GP) *(5)*, standard Spectral Analysis (SA) *(6)*, and rank-shaping spectral analysis (RSSA) *(7)*. The SA β_j grid was defined by 100 components for a reversible ligand with a logarithmic spectral range of 0.01 to 1 (1/min). The RSSA β_j grid was defined by 100 components, the logarithmic spectral range was 0.0001 to 1 (1/min), and the signal-to-noise ratio was [0.01 1].

Parametric imaging: Parametric images were obtained with Logan, MA1, RE-GP, SA and RSSA. For Logan, MA1 and RE-GP, the PET frames used for the regression were chosen on the basis of the start time obtained from the time-activity curve of the whole grey matter. For both spectral analyses, the same parameters used for the analysis at the region level were used to generate the parametric maps. Final V_T values were obtained by averaging the values in the voxels within each region.

Kinetic modeling was performed with Pmod (Pmod Technologies, Zurich, Switzerland) and spectral analysis with SAKE *(8)*.

Quantification of ^{18}F-FIMX binding: Results

Noncompartmental Analyses: At the region level, the V_T results obtained with all alternative techniques, i.e. Logan, Ichise's MA1, MA2, RE-GP, standard SA, and RSSA, were similar to those obtained by the reference two-tissue compartment model method ($p>0.05$; factorial repeated measures ANOVA using Bonferroni adjustment, $F_{1.95,19.54} = 171.7$). Compared to two-tissue compartment model-V_T values, the highest bias (calculated as the average among all brain regions except the cerebellum) was from RSSA (-1.5%). The cerebellum was underestimated to a variable degree with all techniques, ranging from -3.6% for MA2 to -19.7% for RSSA (Supplemental Table 2).

At the voxel level, most techniques replicated the strong results obtained at the region level. The V_T results obtained with RE-GP and SA did not statistically differ from those obtained with a two-tissue compartment model, with an average bias for brain regions (excluding the cerebellum) of -2.1% for RE-GP and -3% for SA ($p>0.05$). However, SA parametric calculations yielded many outlying voxels (whose value was 0) randomly scattered across the brain (Fig 3), which had to be excluded to calculate the average regional values. In addition, in one subject, the SA parametric map yielded only random noise. The SA-V_T average values were thus calculated without including this subject. Logan and MA1 provided only a small bias (-6.5% and -3.5%, respectively), which was nevertheless statistically different from the two-tissue compartment model-V_T ($p<0.05$). RSSA yielded poor results, with an average bias across brain regions of -33%. All techniques underestimated the V_T of the cerebellum to a variable degree, ranging from -14% for RE-GP to about -74% for RSSA.
In summary, all alternative techniques were consistent with a two-tissue compartment model at the region level. At the voxel level, the two SA techniques yielded poor results.

Bloodless quantification: Methods

SRTM: The analyses were performed using either the caudate or the brainstem as reference regions, since the concentration of mGluR1 in these regions has been reported to be very low *(9, 10)*. SRTM allows the calculation of the binding potential over a nondisplaceable compartment (BP_{ND}) *(11)*

SUVR and SUV: The SUV of each brain region was divided by the SUV of the brainstem or the caudate, used as pseudo-reference regions. We calculated the average SUVR from 30-minute intervals of scan data, starting at 10 minutes (i.e. 10-40, 20-50 …, 90-120). In order to assess the optimal time to measure the SUV, we performed a linear regression between two-tissue compartment model-V_T regional values and the SUVR or SUV intervals in the corresponding regions. The analysis for receptor density had to exclude the cerebellum, because its kinetics were much slower than that of the other regions.

Bloodless quantification: Results

The use of a reference region in brain is perhaps the most common bloodless method to quantify receptors in brain. Using the SRTM method, BP_{ND} values obtained using the caudate as a reference region had a lower coefficient of variation than those using the brainstem (19.8% *vs*. 27.6%). However, even using the caudate, the BP_{ND} estimate did not

usually converge in low-binding regions and occasionally showed aberrant values or did not converge for other cortical regions.

As an alternative to SRTM, we examined brain uptake itself (i.e., SUV) and the ratio of uptake in two regions (i.e., SUVR). To determine the optimal time interval, we correlated these parameters of varying 30 min intervals (i.e., 10-40, 20-50…, 90-120 min) with V_T of that region, considered the 'gold standard' for this analysis. The correlation for the optimal time interval (50-80 min) was very good both for SUV (R^2 = 0.989, p <0.0001) and for SUVR (R^2 = 0.983, p <0.0001; using the caudate as the reference region and R^2 = 0.988, p <0.0001 using the brainstem) (Supplemental Fig 2). The 50-80-minute SUVR measured by taking the caudate yielded however the lowest coefficient of variation among all techniques (9.9%) (Supplemental Table 3). Thus, either SUV_{50-80} or $SUVR_{50-80}$ might be used as a bloodless substitute for V_T. With regard to SUVR, however, the reference region (caudate) had a relatively high percentage of specific receptor binding. Thus, the use of $SUVR_{50-80}$ (but not of SUV_{50-80}) would first require showing that V_T in this pseudoreference region does not differ between groups (e.g., patients and controls) or between conditions (e.g., baseline and after receptor blockade).

Receptor Blockade in Monkey: Methods

To measure the nondisplaceable uptake of ^{18}F-FIMX in monkey, we performed a baseline scan and one after complete receptor blockade. A 14-kg male rhesus monkey (*Macaca mulatta*) was imaged with ^{18}F-FIMX at baseline (injected activity: 178 MBq; specific activity: 49.5 GBq/μmol) and after pharmacological blockade (174 MBq; 30.4 GBq/μmol). Pharmacological blockade of mGluR1 was achieved by pre-injection of JNJ16259685 (3 mg/kg). Anesthesia was started with ketamine (10 mg/kg; i.m.) and maintained with 1−3% isoflurane and 98.4% oxygen. Head position was fixed with a stereotactic frame. The monkey was handled in accordance with the *Guide for the Care and Use of Laboratory Animals* and National Institute of Health Animal Care and Use Committee guidelines. The ^{18}F-FIMX bolus (>99% radiochemical purity) was injected through an intravenous perfusion line filled with saline (0.9% w/v). Dynamic PET images of the brain were obtained for up to 180 minutes using a microPET Focus F220 scanner (Siemens Medical Solutions Inc.; Knoxville, TN), with frames of increasing duration from 30 seconds to five minutes. PET images were corrected for attenuation and scatter and reconstructed using Fourier rebinning plus two-dimensional filtered back-projection. PET images were coregistered to a standardized monkey MRI template using SPM8 (Wellcome Trust Centre; London, UK) and the time-activity curves were obtained from a predefined atlas of volumes of interest overlapping several brain regions (frontal cortex, anterior cingulum, striatum, temporal, parietal, and occipital cortex, hippocampus, thalamus, and cerebellum). During both baseline and pre-blocked scan, serial blood samples were manually drawn from a catheter placed in the femoral artery. The samples were centrifuged to obtain the total plasma activity and then analyzed with radio-HPLC to separate the parent from its radiometabolites. The f_P was measured as described for the human studies.

V_T values were calculated using a two-tissue compartment model. Time-stability was assessed by progressively truncating the dynamic scan. The V_{ND} values were measured from the blocked study and also estimated with a Lassen plot.

Receptor Blockade in Monkey: Results

The plasma concentrations peaked about one minute after injection (17 SUV for the baseline and 21 SUV for the blocked scan), and then decreased following a tri-exponential function (Supplemental Figure 3). At least five radiometabolites were observed in plasma that appeared to be less lipophilic than the parent radioligand. The time-activity curves peaked at about 12 minutes and the ^{18}F-FIMX uptake was consistent with the known biodistribution of mGluR1 in mammals: the uptake was high in the cerebellum (7 SUV), intermediate in the thalamus (4 SUV), and lowest in the striatum (3 SUV). The brain time-activity curves were well fitted by a two-tissue compartment model and yielded V_T values ranging from 24.1 mL · cm^{-3} in the cerebellum to 3.5 mL · cm^{-3} in the striatum. V_T in the different brain regions was remarkably stable over time (<5% change from 100 to 180 minutes in all regions, including the cerebellum), which suggests that there were no radiometabolites entering the brain. As in the human studies, BP_{ND} using the striatum as a reference region showed poor time-stability (data not shown), and therefore should not be used to quantify ^{18}F-FIMX.

After blocking, V_T decreased uniformly across the brain regions to 1.52 ± 0.08 mL · cm^{-3}. A Lassen plot yielded a very similar estimation of V_{ND} (x-intercept: 1.57 mL · cm^{-3}; Supplemental Fig 4). The specific binding ranged from 94% for the cerebellum to 54% for the striatum.

The f_P was measured at 0.64% for the baseline scan and 0.89% for the blocked scan. Consequently, V_{ND}/f_P was about 170 mL · cm^{-3}. Since the average f_P in humans is 0.34% and the estimated V_{ND} is 0.5 mL · cm^{-3}, the V_{ND}/f_P in humans was about 150 mL · cm^{-3}, thus confirming that the non-specific binding was similar between human and non-human primates.

Whole-body biodistribution and dosimetry: Methods

To determine the radiation exposure to organs of the body, four healthy subjects (two men and two women, 31 ± 14 y; 62 ± 8 kg) underwent a whole-body scan after injection of 193 ± 3.8 MBq of ^{18}F-FIMX to complete the dosimetry assessment. Whole-body imaging was performed by dynamic scanning of the body (from the head to mid-thigh) in seven contiguous segments, as described elsewhere *(12)*. All PET scans were performed with an Advance tomograph (GE Healthcare), which was equipped with an external ^{68}Ge source used for attenuation correction. The MRI was a 3 T Achieva (Philips Health Care).

The organs with the highest uptake visible on the PET images (brain, lungs, heart, liver, gallbladder, spleen, kidneys, urinary bladder, and lumbar vertebrae) were manually delineated to be used as source organs. The uptake in the source organs was corrected with a recovery coefficient based on the averaged activity of the frames of the whole body dynamic scan using large regions of interest drawn semi-automatically around the body. The average recovery coefficient of the four subjects was 90%. The radioactivity concentration, measured without decay correction, was expressed as a percentage of injected activity for each organ. The organ residence times were calculated as the areas under the time activity curve for each organ by using the trapezoidal rule and by physical decay after the last frame. Because the total red marrow present in the lumbar vertebrae is 11.7% of the mass of red marrow in the whole body *(13)*, the red marrow final residence time was obtained by dividing the residence time in the lumbar vertebrae by 0.117. The accumulation over time of the radioactivity in the urinary bladder (expressed as cumulative % of the injected activity) was fitted with a monoexponential function to obtain the parameters for the dynamic bladder model. The fitting indicated that, on average, 56% of injected activity was excreted

via the urine at infinite time, with a biological half-life of 0.68 hours. A voiding interval of 2.4 hours was assumed. To obtain the residence time for the remainder of the body, the residence times of all source organs were summed and then subtracted from the theoretical value of 2.64 hours (^{18}F half-life/ln2). The residence times were entered into OLINDA/EXM 1.1 *(14)* to calculate dosimetry values using the adult male anthropomorphic phantom.

Whole-body biodistribution and dosimetry: Results

After early accumulation in organs with high blood volume (heart, kidneys), the radioactivity was excreted via both hepatobiliary and urinary routes (Supplemental Fig 5). The brain had high radioactivity uptake, with a peak of about 8% of the injected activity four to eight minutes after injection. The liver and the gallbladder were the organs with the longest residence times (0.226 and 0.121 hours, respectively) (Supplemental Table 4). The highest exposure was found in excretory organs such as the bladder (251 μSv/MBq), the gallbladder (245 μSv/MBq), and the kidneys (42 μSv/MBq) (Supplemental Table 5). The effective dose was 23.4 μSv/MBq on average, with a small range among the four subjects (23.3 to 23.5 μSv/MBq).

Supplemental References

1. Zoghbi SS, Shetty HU, Ichise M, et al. PET imaging of the dopamine transporter with ^{18}F-FECNT: a polar radiometabolite confounds brain radioligand measurements. *J Nucl Med.* 2006;47(3):520-527.

2. Zanotti-Fregonara P, Lammertsma AA, Innis RB. Suggested pathway to assess radiation safety of (1)(8)F-labeled PET tracers for first-in-human studies. *Eur J Nucl Med Mol Imaging.* 2013;40(11):1781-1783.

3. Logan J, Fowler JS, Volkow ND, et al. Graphical analysis of reversible radioligand binding from time-activity measurements applied to [N-^{11}C-methyl]-(-)cocaine PET studies in human subjects. *J Cereb Blood Flow Metab.* 1990;10:740-747.

4. Ichise M, Toyama H, Innis RB, Carson RE. Strategies to improve neuroreceptor parameter estimation by linear regression analysis. *J Cereb Blood Flow Metab.* 2002;22(10):1271-1281.

5. Zhou Y, Ye W, Brasic JR, Wong DF. Multi-graphical analysis of dynamic PET. *Neuroimage.* 2010;49(4):2947-2957.

6. Cunningham VJ, Jones T. Spectral-Analysis of Dynamic Pet Studies. *J Cereb Blood Flow Metab.* 1993;13(1):15-23.

7. Turkheimer FE, Hinz R, Gunn RN, Aston JAD, Gunn SR, Cunningham VJ. Rank-shaping regularization of exponential spectral analysis for application to functional parametric mapping. *Phys Med Biol.* 2003;48(23):3819-3841.

8. Veronese M, Rizzo G, Turkheimer FE, Bertoldo A. SAKE: A new quantification tool for positron emission tomography studies. *Comput Methods Programs Biomed.* 2013;111(1):199-213.

9. Spooren W, Ballard T, Gasparini F, Amalric M, Mutel V, Schreiber R. Insight into the function of Group I and Group II metabotropic glutamate (mGlu) receptors: behavioural characterization and implications for the treatment of CNS disorders. *Behav Pharmacol.* 2003;14(4):257-277.

10. Stephan D, Bon C, Holzwarth JA, Galvan M, Pruss RM. Human metabotropic glutamate receptor 1: mRNA distribution, chromosome localization and functional expression of two splice variants. *Neuropharmacology.* 1996;35(12):1649-1660.

11. Lammertsma AA, Hume SP. Simplified reference tissue model for PET receptor studies. *Neuroimage.* 1996;4:153-158.

12. Brown AK, Fujita M, Fujimura Y, et al. Radiation dosimetry and biodistribution in monkey and man of 11C-PBR28: a PET radioligand to image inflammation. *J Nucl Med.* 2007;48(12):2072-2079.

13. Cristy M. Active bone marrow distribution as a function of age in humans. *Phys Med Biol.* 1981;26(3):389-400.

14. Stabin MG, Sparks RB, Crowe E. OLINDA/EXM: the second-generation personal computer software for internal dose assessment in nuclear medicine. *J Nucl Med.* 2005;46(6):1023-1027.